Sensorless Control of High-Speed Surface Permanent Magnet Synchronous Motors for Enhanced Dynamic Performance

Shun Lan. Student member[1], Jian Li. Senior member[2]
[1] Huazhong University of Science and Technology, China
[2] Huazhong University of Science and Technology, China

***Abstract*-- This paper presents an advanced sensorless control technique for high-speed surface permanent magnet synchronous motors (SPMSMs) under low switching-to-fundamental frequency ratios. The algorithm proposed aims to enhance the dynamic performance of the system while simultaneously ensuring robust steady-state characteristics. The paper begins by addressing the challenges associated with rapid control of high-speed motors. Next, the proposed algorithm is presented in detail, highlighting the use of direct eigen control which utilize the eigen-based discrete model of SPMSM and sliding mode observers to achieve high dynamic performance without the need for position sensors. The effectiveness of the proposed algorithm is demonstrated through simulation and experiment.**

***Index Terms*—SPMSM, deadbeat predictive control, sliding mode observer**

I. INTRODUCTION

High-speed surface permanent magnet synchronous motors (SPMSMs) have become increasingly popular in various industrial applications, such as flywheel energy storage system and hydraulic pump, due to their high-power density and efficiency [1]. However, achieving high rapid control and steady-state performance of high-speed SPMSMs is a challenging task due to the nonlinearity, uncertainty, and time-varying characteristics of these motors, especially when the ratio of the switching frequency to the machine frequency is low. Traditional control methods, such as field-oriented control (FOC) [2], are widely used for SPMSMs but the dynamic performance is limited. Furthermore, the use of position sensors to measure rotor position and velocity has limitations such as additional cost, complexity, and potential reliability issues. Therefore, there is a growing interest in the development of sensorless control methods that can achieve accurate and efficient control of SPMSMs without relying on position sensors.

Predictive control is a type of advanced control strategy that uses a mathematical model of the system to predict future behavior and optimize the control input, which shows better steady and dynamic performance, and it has captured considerable attention. Predictive control can be mainly classified into two categories: model predictive control (MPC) and deadbeat predictive control (DPC) [3]. DPC is computationally efficient and is especially suitable for systems with fast dynamics, the proposed method leverages this concept and possesses the characteristics of this approach. The sensorless control methods for SPMSM can be broadly classified into two categories: one is based on the saliency in the spatial impedance of the motor at standstill or low-frequency operation, while the other is based on the electromotive force (EMF) in the middle and high-speed regions, which uses voltage models and observers in the synchronous or stationary frame [4]. This paper focused on dealing with the control issues in the middle and high-speed regions.

Several authors have employed the deadbeat control strategy in the sensorless control region. In [5], Zhao et al. employed a hybrid control strategy [5], comprising a deadbeat controller and an extended state observer, to enhance the control performance at low speeds. Jiang et al. [6] adopted deadbeat-based predictive current control scheme and the sliding mode control strategy which shows strongly robust to acute variation of load. However, the dynamic performance of the system was found to be insufficiently rapid. Ton et al. [7] present a deadbeat direct-current and flux linkage control scheme with speed estimation combined with LPF to achieve the high dynamic control of SPMSM. Nevertheless, the delay induced by LPF leads to spikes and ringing in the torque output.

In this paper, a direct eigen control strategy according to the eigen-based discrete-model is proposed, which shows high model accuracy under low switching-to-fundamental frequency ratios, and a super twist sliding mode observer is adopted for sensorless control. The paper is organized as follows. Section II deduces the eigen-based model for SPMSM, which exhibits exceptional accuracy in terms of modeling and then the direct eigen control strategy is designed utilizing Karman filter. Section III adopts the SMC to estimate the EMF and a Luenberger speed observer is utilized to obtain improved performance in flux position and motor speed estimate. Finally, in order to validate the effectiveness of the algorithm., simulation is carried out on a test motor, and a test bench experiment is also conducted on the motor.

II. DIRECT EIGEN CONTROL OF SPMSM

Direct eigen control require a high-precision discretized model of motor to predict the current of the next time step and calculate the voltage.

A. Eigen-based model of SPMSM

The circuit model of SPMSM can be described by stator voltage complex vector, stator current complex vector, and the rotor flux complex vector in the following vector equation:

$$\mathbf{V}_s = R_s \mathbf{I}_s + L_s \frac{d\mathbf{I}_s}{dt} + \frac{d\boldsymbol{\psi}_r}{dt} \tag{1}$$

Where R_S is the stator resistor and L_S is the stator inductance of SPMSM.

Selecting the stator current complex vector and rotor flux complex vector as the state variables, the state equation of SPMSM is shown in (2):

$$\dot{X} = AX + BU \tag{2}$$

The corresponding state vector, state matrix, input matrix, input vector is as (3), where $\alpha = R_s/L_s, \beta = 1/L_s$, and i is imaginary operator.

$$\begin{aligned} X &= \begin{bmatrix} I_s \\ \psi_r \end{bmatrix}, A = \begin{bmatrix} -\alpha & -i\omega\beta \\ 0 & i\omega \end{bmatrix} \\ B &= \begin{bmatrix} \beta \\ 0 \end{bmatrix}, U = V_s \end{aligned} \tag{3}$$

The exact solution of equation (2) is:

$$X(t) = e^{At}X(0) + \int_0^t e^{A(t-\tau)}BU(\tau)d\tau \tag{4}$$

In the discrete-time system, assuming the sampling time step is T, then the state at time $t_n + \mathrm{T}$ can be calculated by the following equation from the state at time t_n, as:

$$X(t_n + T) = FX(t_n) + GV \tag{5}$$

F is the transition matrix, is the input matrix and V is the mean control Vector, and through mathematical computations, they can be calculated by the state matrix A, the input matrix B and the input vector U in the continuous-time system and the unit matrix I as:

$$F = e^{AT}, G = A^{-1}(e^{AT} - I)B, V = \frac{1}{T}\int_{t_n}^{t_n+T} U(\tau)d\tau \tag{6}$$

It is shown that the matrix exponential e^{AT} is the key to obtain the exact solution of the transition matrix F and input matrix G. There are several methods to calculate the matrix exponential: Taylor series, Laplace transform and diagonalization. The diagonalization which calculates the exponential by exponentiating its eigenvalues and using them to construct a diagonal matrix is more efficient and accurate. As a result, the eigen-based method is adopted in this paper.

The eigenvalues $\lambda_{\mathrm{i}}, (\mathrm{i} = 1,2)$, are calculated through:

$$\det(\lambda_i I - A) = 0 \tag{7}$$

And the diagonalized matrix D constructed by eigenvalues is:

$$D = \begin{bmatrix} \lambda_1 & 0 \\ 0 & \lambda_2 \end{bmatrix} = \begin{bmatrix} -\alpha & 0 \\ 0 & i\omega \end{bmatrix} \tag{8}$$

The transfer matrix P constructed by the eigenvectors corresponding to each eigenvalue is:

$$P = \begin{bmatrix} 1 & 1 \\ 0 & -\dfrac{\lambda_2 - \lambda_1}{\lambda_2 \beta} \end{bmatrix} = \begin{bmatrix} 1 & 1 \\ 0 & -\dfrac{1}{\chi} \end{bmatrix} \tag{9}$$

By defining the variable χ, the expression of transfer matrix could be simplified. Finally, the transition matrix and F the input matrix G can be calculated by equation (10) and (11).

$$F = e^{AT} = Pe^{DT}P^{-1} = \begin{bmatrix} e^{\lambda_1 T} & \chi(e^{\lambda_1 T} - e^{\lambda_2 T}) \\ 0 & e^{\lambda_2 T} \end{bmatrix} \tag{10}$$

$$G = PD^{-1}(e^{DT} - I)P^{-1}B = \begin{bmatrix} \beta \dfrac{e^{\lambda_1 T} - 1}{\lambda_1} \\ 0 \end{bmatrix} \tag{11}$$

B. Direct eigen control process of SPMSM

The voltage command generated by the controller will be applied in the next sampling period, resulting in an inherent delay of one beat. To eliminate this beat delay, the deadbeat controller calculates the voltage command that will be applied in the next beat in the current sampling period. The deadbeat control process is shown in Fig. 1, which starts by sampling the current and at time $t_n - T$, and then predict the motor's state at time t_n as shown in equation (12), the subscript p represents the predicted value

$$X_p(t_n) = F(t_n - T)X(t_n - T) + G(t_n - T)V_{t_n - T \to t_n} \tag{12}$$

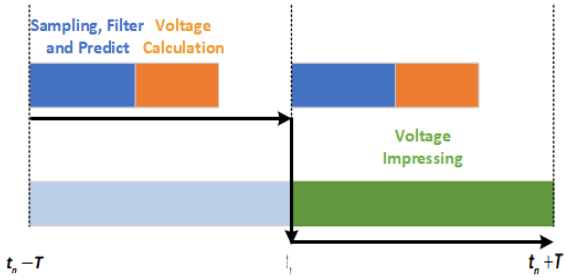

Fig. 1. Timing sequence of direct eigen control process

Then the predicted state is employed to compute the voltage applied during the interval from time t_n to $t_n + T$ as shown in (13) where the subscript s represents the set value. To simplify the voltage calculations, a coordinate

transformation is required. In the dq coordinate system, the state vector can be rewritten as Equation 14.

$$\begin{bmatrix} 1 & \chi \\ 0 & -\chi \end{bmatrix} X_s(t_n+T) = \begin{bmatrix} e^{\lambda_1} & 0 \\ 0 & e^{\lambda_2} \end{bmatrix} \begin{bmatrix} 1 & \chi \\ 0 & -\chi \end{bmatrix} X_p(t_n) + \begin{bmatrix} \beta \dfrac{e^{\lambda_1 T}-1}{\lambda_1} \\ 0 \end{bmatrix} V \tag{13}$$

$$X_{(d,q)} = \begin{bmatrix} I_d + iI_q & \psi_r \end{bmatrix}^T \tag{14}$$

However, at times $t = t_n$ and $t = t_n + T$ their dq-axis positions are different. Here, the dq-axis positions at time $t = t_n$ and at time $t = t_n + T$ are denoted as d_0, q_0 and d, q to respectively. the d-axis angle at time $t = t_n$ is represented by θ_0, whereas at time $t = t_n + T$, it assumes the value of θ.

The mechanical time constant is much larger than the electrical time constant. Within the time interval T, it is reasonable to assume that the angular velocity ω remains constant. As a result, the relationship between the two axis angles can be expressed as Equation 15：

$$\theta = \theta_0 + \omega T \tag{15}$$

Figure 2 illustrates the relationship between different axes

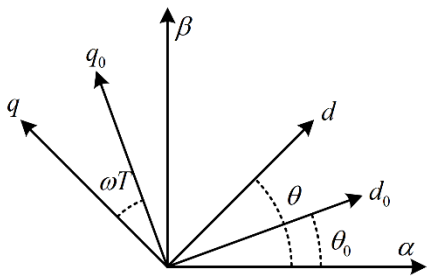

Fig. 2. The relationship between the axes

Equation 13 can be rewritten as follows:

$$\begin{bmatrix} 1 & \chi \\ 0 & -\chi \end{bmatrix} e^{i\theta} X_{s(d,q)} = \begin{bmatrix} e^{\lambda_1} & 0 \\ 0 & e^{\lambda_2} \end{bmatrix} \begin{bmatrix} 1 & \chi \\ 0 & -\chi \end{bmatrix} e^{i\theta_0} X_{p(d_0,q_0)} + \begin{bmatrix} \beta \dfrac{e^{\lambda_1 T}-1}{\lambda_1} \\ 0 \end{bmatrix} V_{(\alpha,\beta)} \tag{16}$$

define the variable $\xi = I_d + iI_q + \chi\psi_r$, we can get:

$$e^{i\theta}\xi_s = e^{\lambda_1 + i\theta_0}\xi_p + \beta \frac{e^{\lambda_1 T}-1}{\lambda_1} V_{(\alpha,\beta)} \tag{17}$$

Finally, the voltage reference can be calculated as:

$$V_{(\alpha,\beta)} = e^{i\theta} \frac{e^{\lambda_2 T}\xi_s - e^{\lambda_1 T}\xi_p}{\beta(e^{\lambda_1 T}-1)} \lambda_1 \tag{18}$$

C. Karman filter

Theoretically, employing the aforementioned control process enables the actual state values to converge towards the desired setpoints. However, in practical operation, current sampling is influenced by disturbances, and mismatch in motor parameters can lead to deviations between the calculated voltage commands and the ideal values. Furthermore, the presence of deadtime and inverter nonlinearity effects introduces discrepancies between the output voltage and the desired voltage commands. Consequently, deviations between the actual state values and the desired setpoints arise. An effective method to reduce state deviations is to introduce a Kalman filter, which performs reprocessing on the actual state.

The current vector I_s is chosen here as the measured variable Y_m , the subscript m denotes the measured value. The relationship between Y and state variables X is as shown in (19), and $H = [1 \quad 0]$

$$Y = HX \tag{19}$$

The filtering value can be obtained by using the measured variable and the predicted state and variable from the previous beat through (20):

$$X_f(t_n - T) = X_p(t_n - T) + K\left(t_n - T\right) \{Y_m(t_n - T) - Y_p(t_n - T)\} \tag{20}$$

K is the Kalman gain which determines whether the current value of the filtered state variable is closer to the predicted value or the measured value. And the corresponding calculation process is as follows:

$$\begin{aligned} P_p(t_n) &= F * P(t_n - T) * F^t + Q_0 \\ K(t_n) &= P_p(t_n) H^t \{H * P_p(t_n) * H^t + R_0\}^{-1} \\ P(t_n) &= \{1 - K(t_n) * H\} * P_p(t_n) \end{aligned} \tag{21}$$

P is the state error covariance matrix, Q_0 is the state disturbance covariance matrix, R_0 is the measurement disturbance covariance matrix. The aforementioned process yields the coefficient matrix K that minimizes the combined measurement error and prediction error. After processing through the Kalman filter, Equation 12 is rewritten as Equation 22:

$$X_p(t_n) = F(t_n - T) X_f(t_n - T) + G(t_n - T) V_{t_n - T \to t_n} \tag{22}$$

III. FLUX POSITION OBSERVE

The estimation of back electromotive force (EMF) using a first-order sliding mode observer is prone to chattering. A low-pass filter can be used to reduce chattering, but it may also lead to a decrease in the system's dynamic response. Replacing the sign function can improve the performance, but a filter is still required to extract the EMF information. On the other hand, high-order sliding mode observers can effectively suppress chattering without the need for a filter. As a result, a super-twisting algorithm-based sliding mode observer (STA-SMO) is adopted in this paper to achieve high dynamic and accuracy position estimation. The STA-SMO is constructed as equation (23):

$$\begin{aligned}\frac{d\hat{i}_\alpha}{dt} &= -\frac{R}{L}\hat{i}_\alpha + \frac{1}{L}u_\alpha + \frac{k_1}{L}\left|\bar{i}_\alpha\right|^{1/2} sign(\bar{i}_\alpha) + \int \frac{k_2}{L} sign(\bar{i}_\alpha)dt \\ \frac{d\hat{i}_\beta}{dt} &= -\frac{R}{L}\hat{i}_\beta + \frac{1}{L}u_\beta + \frac{k_1}{L}\left|\bar{i}_\beta\right|^{1/2} sign(\bar{i}_\beta) + \int \frac{k_2}{L} sign(\bar{i}_\beta)dt\end{aligned} \tag{23}$$

Subtracting Equation (1) from Equation (23), we obtain the current error equation as shown in (24):

$$\begin{aligned}\frac{d\bar{i}_\alpha}{dt} &= -\frac{R}{L}\bar{i}_\alpha + \frac{1}{L}e_\alpha + \frac{k_1}{L}\left|\bar{i}_\alpha\right|^{1/2} sign(\bar{i}_\alpha) + \int \frac{k_2}{L} sign(\bar{i}_\alpha)dt \\ \frac{d\bar{i}_\beta}{dt} &= -\frac{R}{L}\bar{i}_\beta + \frac{1}{L}e_\beta + \frac{k_1}{L}\left|\bar{i}_\beta\right|^{1/2} sign(\bar{i}_\beta) + \int \frac{k_2}{L} sign(\bar{i}_\beta)dt\end{aligned} \tag{24}$$

In order to ensure the stable operation of the system, the parameters k_1 and k_2 need to meet the following conditions.

$$k_1 > 2\delta, k_2 > k_1 \frac{5\delta k_1 + 4\delta^2}{2(k_1 - 2\delta)} \tag{25}$$

δ is the parameter that satisfy the globally bounded condition for the system's uncertain term as shown in equation (26):

$$\begin{aligned}\left|\rho_\alpha\right| &= \left|-\frac{R}{L}\bar{i}_\alpha + \frac{1}{L}e_\alpha\right| \le \delta\left|\bar{i}_\alpha\right|^{1/2} \\ \left|\rho_\beta\right| &= \left|-\frac{R}{L}\bar{i}_\beta + \frac{1}{L}e_\beta\right| \le \delta\left|\bar{i}_\beta\right|^{1/2}\end{aligned} \tag{26}$$

Although fixed values of k_1 and k_2 can satisfy the conditions for Lyapunov stability, it is challenging to simultaneously consider the system's dynamics and position observation errors within a wide operating range. Therefore, adaptive sliding mode parameters are utilized here to enhance the system's response capability, which are shown in equation (27). σ_1 and σ_2 are the test coefficients.

By operating at a fixed speed, and under the condition of satisfying Equation 25, the best values for the coefficients σ_1 and σ_2 are determined through a selection process for optimization. The constructure of STA-SMO is shown in Fig. 3.

$$k_1 = \sigma_1\left|\omega\right|, k_2 = \sigma_2\omega^2 \tag{27}$$

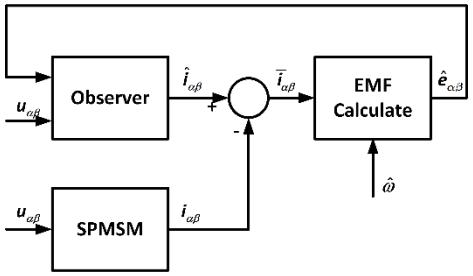

Fig. 3. Constructure of STA-SMO

Due to the presence of the integral term, the estimated back electromotive force (EMF) becomes relatively smooth with appropriate parameter, and the filter can therefore be avoided. By utilizing the estimated back EMF, the angle error information can be obtained using Equation (28):

$$-\hat{E}_\alpha \cos\hat{\theta} - \hat{E}_\beta \sin\hat{\theta} \approx \omega\psi_r(\theta - \hat{\theta}) \tag{28}$$

The Luenberger observer, in conjunction with the normalization, is employed to attain high dynamics of the estimated flux position while utilizing the same observer parameters, which is shown in Fig. 4.

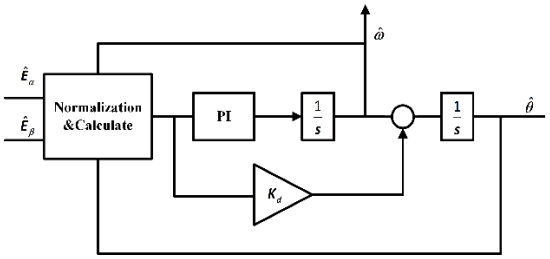

Fig. 4. Position observer

IV. SIMULINK AND EXPERIMENT RESULT

TABLE I
Motor parameter of the experiment motor

Parameter	Value	Parameter	Value
Rated power (kW)	1.5	Stator resistance (Ω)	0.273
Rated speed (rpm)	1500	Stator inductance (mH)	0.0023
Rated torque (Nm)	9.6	Dc Voltage (V)	200
Number of poles	5	Magnetic flux (Wb)	0.1246

To demonstrate the performance of proposed strategy, simulation is carried out on a motor for a test motor, and it is also verified by test bench experiment. The corresponding parameter of the motor is shown in Table 1. The switch frequency of the motor is set to 1 kHz. Due to the use of asymmetric sampling, the sampling frequency is 2 kHz. At lower calculation frequencies, the traditional motor model lacks sufficient discretization accuracy, while the direct eigenvalue-based motor model exhibits

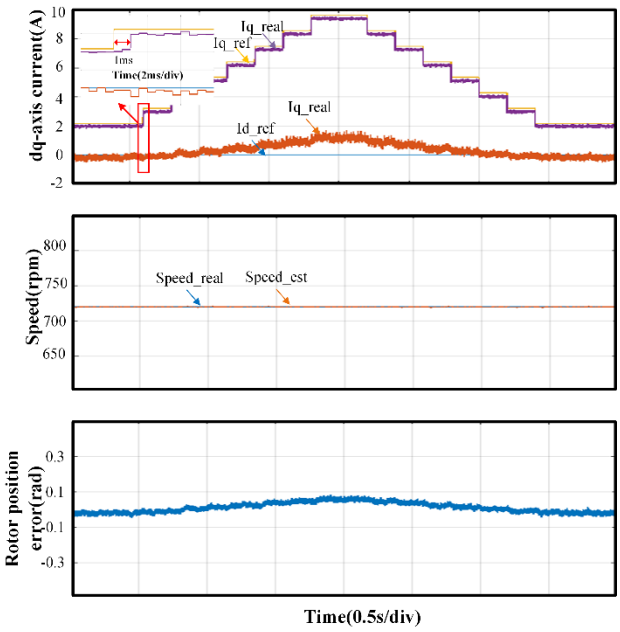

Fig. 5. Load-dynamics simulation.

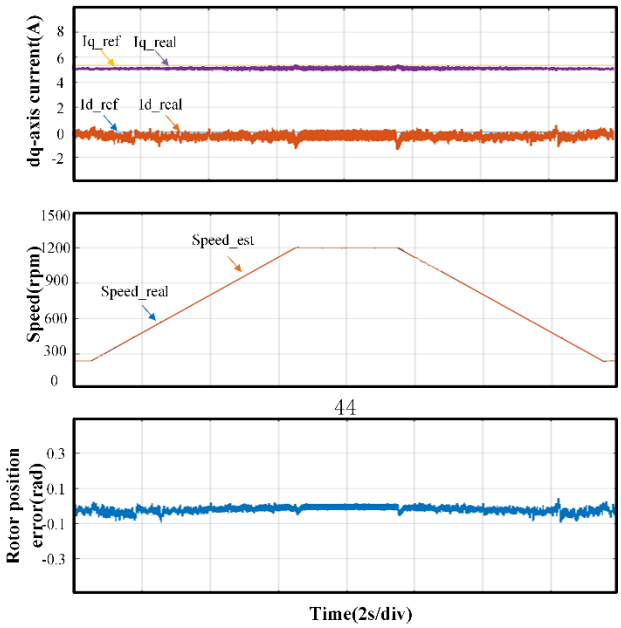

Fig. 6. Speed-dynamics simulation

higher discretization accuracy at this time. Furthermore, sliding mode control requires a higher calculation frequency, so it is performed within the timer interrupt. The timer frequency is set to 20 kHz. To ensure the accuracy of the calculations, voltage reconstruction is necessary. Figure 5 and Figure 6 represent the simulation waveforms of load dynamics and speed dynamics, respectively. From the graphs, it can be observed that the angle error remains within ±5 degrees. From Figure 5, it can be seen that it took 1ms for the actual current to follow the command current, which corresponds to two calculation cycles. This demonstrates strong dynamic response capability. The variation in speed has a minor impact on the angle error, while the load variation has a significant influence on the sliding mode observer. The angle error eventually results in a deviation between the actual d-axis current and the reference current. The angle error is also affected by the bandwidth of position observer. Higher bandwidth reduces steady-state error but worsens

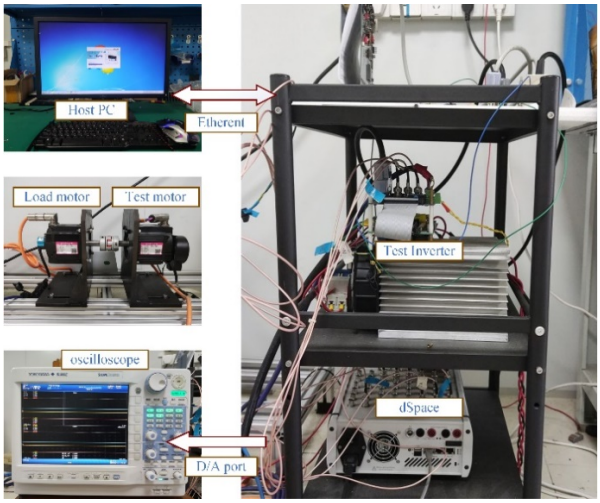

Fig. 7. experiment platform

dynamic response, while lower bandwidth has the opposite effect.

Fig. 7 is the picture of the experiment platform. The algorithm is carried on dSPACE platform and it works in torque mode. The load machine controls the speed. The values of i_d, i_q, ω_r, and θ_{err} are transported through D/A interface of dSPACE and recorded by oscilloscope. In the experiment, the current sampled by the current sensor is susceptible to electromagnetic interference and there exists mismatch between the actual motor parameters and the values used. Furthermore, as the motor operates under different operating conditions, the motor parameters can vary, leading to measurement errors and prediction errors. A Kalman filter is incorporated in the experiment with the aim of minimizing measurement and prediction errors. By adjusting the coefficient matrix K, the magnetic flux magnitude and angle used in the calculations are influenced, ultimately reducing the absolute difference between the current command value and the actual value.

Fig.8 illustrates the corresponding dq-axis currents, angular velocity observed by the position observer, and the variation in the error between the measured motor electrical angle and the estimated angle during load changes under sensorless control. In this scenario, the load motor is controlled at 720 rpm, the actual current tracks the commanded current, achieving high dynamics under sensorless control. When using a Kalman filter, the q-axis actual current becomes closer to the commanded current, reducing the deviation. The d-axis current is minimally affected in this case. During load changes, the flux position error remains within a range of ±5 degrees, and as the torque increases, the mean value of the angle error changes, resulting in a deviation in the d-axis current. Furthermore, in the actual experiment, variations in torque will cause slight changes in motor speed. This can be observed in the graph as well. Fig.9 illustrates the corresponding dq-axis

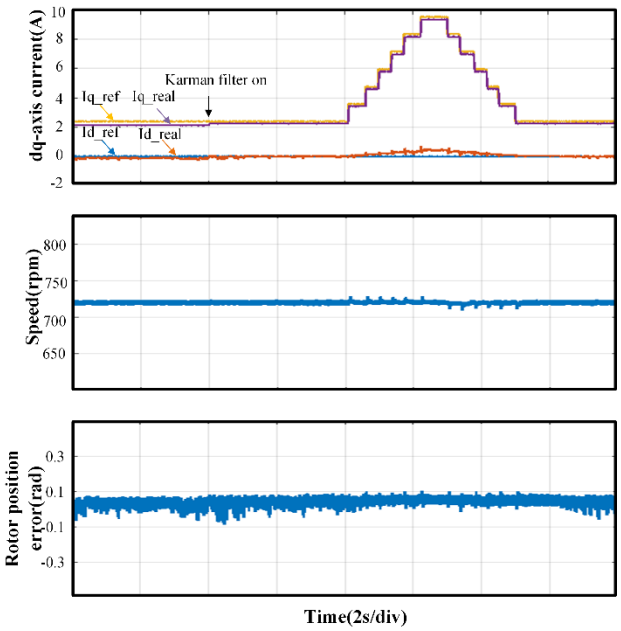

Fig. 8. Load-dynamics experiment.

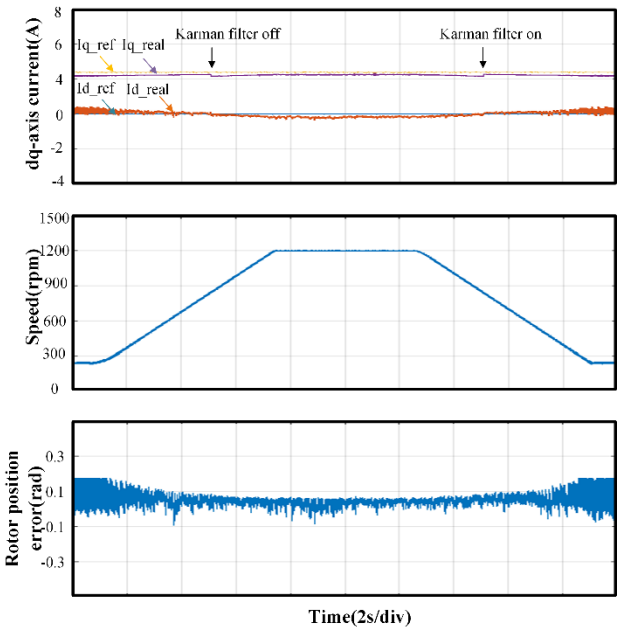

Fig. 9. Speed-dynamics experiment

currents, angular velocity observed by the position observer, and the variation in the error between the measured motor angle and the estimated angle during speed changes. At lower speeds, there exists fluctuation in the estimated speed and the flux position error remains within a range of ±10 degrees, as the speed increase, the fluctuation of position error decrease. In the high speed, the actual q axis current is closer to the reference and the Kalman gain K approaches 1, so there is no need to use a Kalman filter.

V. Conclusions

This paper proposes a deadbeat predictive control based on a direct eigenvalue discretized motor model, which shows higher model precision, and therefore a more accurate voltage reference can be obtained. Besides, the Karman filter is utilized to mitigate the effects of disturbances and model errors. By employing a super-twisting sliding mode controller to observe the speed and rotor position information, which avoid the use of low-pass filters, it achieves high dynamic response control without the position sensors. The efficacy of the algorithm is verified through simulations and experimental validations.

References

[1] P. Pillay and R. Krishnan, "Modeling, simulation, and analysis of permanent-magnet motor drives. I. The permanent-magnet synchronous motor drive," in IEEE Transactions on Industry Applications, vol. 25, no. 2, pp. 265-273, March-April 1989

[2] S. S. Kuruppu, "Position Sensor Harmonics Influence on Highly Integrated Field Oriented Controlled PMSM Drive Torque Output," 2021 IEEE Transportation Electrification Conference & Expo (ITEC), Chicago, IL, USA, 2021, pp. 427-433

[3] R. D. Lorenz, "The emerging role of dead-beat, direct torque and flux control in the future of induction machine drives," 2008 11th International Conference on Optimization of Electrical and Electronic Equipment, Brasov, Romania, 2008, pp. XIX-XXVII

[4] R. B. Sepe and J. H. Lang, "Real-time observer-based (adaptive) control of a permanent-magnet synchronous motor without mechanical sensors," in IEEE Transactions on Industry Applications, vol. 28, no. 6, pp. 1345-1352, Nov.-Dec. 1992

[5] Z. Xue, Z. Chen and G. Luo, "A Novel Deadbeat Control with Extended State Observer for PMSM Sensorless Drive System," 2018 21st International Conference on Electrical Machines and Systems (ICEMS), Jeju, Korea (South), 2018, pp. 1612-1617

[6] Y. Jiang, W. Xu, C. Mu and Y. Liu, "Improved Deadbeat Predictive Current Control Combined Sliding Mode Strategy for PMSM Drive System," in IEEE Transactions on Vehicular Technology, vol. 67, no. 1, pp. 251-263, Jan. 2018

[7] T. -D. Ton and M. -F. Hsieh, "A Simple Model-Based Deadbeat Direct-Current and Flux Linkage Control Scheme for Sensorless SPMSM Drive," 2021 IEEE International Future Energy Electronics Conference (IFEEC), Taipei, Taiwan,2021, pp.1-6